Available online at www.sciencedirect.com
SCIENCE DIRECT®
Journal of Solid State Chemistry 177 (2004) 2499–2505
JOURNAL OF SOLID STATE CHEMISTRY
http://elsevier.com/locate/jssc

Synthesis, structure and properties of $CsHSi_3O_7$, a layered silicate with a chiral structure

Xiqu Wang,* Lumei Liu, Jin Huang, and Allan J. Jacobson

Department of Chemistry and Center for Materials Chemistry, University of Houston, Houston, TX 77204-5003, USA

Received 3 November 2003; received in revised form 4 February 2004; accepted 4 April 2004

Abstract

The chiral layered silicate $CsHSi_3O_7$ has been synthesized by hydrothermal techniques, and its structure determined by single crystal X-ray diffraction. The compound crystallizes in the space group $P2_12_12_1$. The silicate single layer consists of both four- and three-connected SiO_4 tetrahedra and may be considered as a member of a series of layer structures with the general formula $(Si_4O_9)_m(Si_2O_5)_n$. Strong hydrogen bonds occur between the terminal OH^- and O^{2-} ions of neighboring layers. The Cs^+ cations can be ion-exchanged by protons to give a phase of composition $H_2Si_3O_7 \cdot H_2O$ with a water molecule occupying the original Cs position, as confirmed by single crystal X-ray diffraction data. The water molecule in $H_2Si_3O_7 \cdot H_2O$ can be readily removed without collapse of the crystal structure. Both $CsHSi_3O_7$ and $H_2Si_3O_7 \cdot H_2O$ show SHG (second harmonic generation) efficiencies comparable to that of quartz, and both are not phase-matchable materials.
© 2004 Elsevier Inc. All rights reserved.

Keywords: Cesium silicate; Layered silicate; Chiral structure; Hydrothermal synthesis; Ion-exchange

1. Introduction

Many layered silicates can incorporate functional species in their interlayer space to form nanocomposite materials. The interlayer space serves as a platform of nanometer scale for constructing new materials or tuning material properties by chemical means such as intercalation [1–4]. Organization of the intercalated species is decided by the structure and composition of the host layered lattice. The host lattice usually expands perpendicular to the layers to accommodate the guest species and the layer structure is largely preserved. Layered lattices with non-centrosymmetry are particularly interesting because they can align functional species in a preferred orientation, which is a prerequisite for important physical properties such as non-linear optical activity [5,6]. A prominent example is the recent report of an acentric arrangement of *p*-nitroaniline molecules intercalated between the layers of kaolinite. The second harmonic generation (SHG) intensity observed for the intercalated hybrid material was found to be substantially higher than that for the original kaolinite host [7]. Layered silicates have also been used for constructing nanoporous materials by metal oxide pillaring or by grafting alkoxysilyl groups [8–10]. In this aspect, chiral layer lattices are ideal starting points for constructing porous frameworks with chiral symmetry that have potential applications in separations of chiral molecules.

A large number of layered silicates are known and well characterized, though silicates with chiral layered structures are very rare [11–15]. We have been interested in synthesis of microporous materials based on linking silicate layers with other structural units, particularly with transition metal cations [16–18]. As a result of a systematic synthesis study of the effect of reactant composition in $CsOH$–SiO_2–transition metal oxide systems using hydrothermal techniques, we obtained a new alkali metal silicate $CsHSi_3O_7$ that has a layered chiral structure.

*Corresponding author. Fax: +713-743-2780.
E-mail address: xiqu.wang@mail.uh.edu (X. Wang).

0022-4596/$ - see front matter © 2004 Elsevier Inc. All rights reserved.
doi:10.1016/j.jssc.2004.04.013

2. Experimental

2.1. Synthesis

Fumed silica (1.3 g, Aldrich, surface area 380 m^2/g) preheated at 110°C for 2 h, was dissolved in aqueous CsOH (4.3 ml, 4.24 M, Aldrich). The solution was diluted by adding 1.3 ml deionized water. The pH value of the diluted solution was adjusted to 13.6 with concentrated nitric acid (Merck, 68–70 wt%). The clear solution was subsequently sealed in a Teflon lined Parr autoclave (23 ml inner volume) and heated at 225°C for 3 d under autogenous pressure. After cooling over 4 h the product was recovered by vacuum filtration and washed with water and methanol. The final solution pH was ~11.6. Colorless platy crystals of $CsHSi_3O_7$ were obtained as a single phase with a maximal crystal size of ca. 0.2 mm. The yield is >80% based on silica.

2.2. Characterization

The crystals were analyzed by EDX using a JEOL JSM 6400 scanning electron microscope with a Link Analytical EXL spectrometer. A Cs:Si atomic ratio close to 1:3 was obtained in agreement with crystal structure refinements. Chemical analyses of the proton ion-exchanged samples were made at Galbraith Laboratories, Knoxville, TN. Thermogravimetric analysis (TGA) was carried out on a TA Instruments Hi-Res 2950 system with a heating rate of 5°C/min in flowing dry N_2 after initially equilibrating the sample at 30°C for 20 min to remove any surface water. Infrared spectra were collected with a Galaxy FTIR 5000 spectrometer using the KBr pellet method in air. To remove surface water, the samples were measured immediately after heating at 50°C for 20 min. UV-Vis-NIR diffuse reflectance spectra were measured with a Cary 500 spectrophotometer on powder samples at room temperature. Powder XRD data were recorded on a SCINTAG XDS2000 automated diffractometer with CuK_α radiation at room temperature with flat plate samples.

2.3. Ion-exchange

Proton ion-exchange experiments were carried out by stirring powder samples in a large excess of 1 M nitric acid at 100°C for 2 d, followed by washing with de-ionized water. Ion-exchanged single crystals were prepared in a similar way but extending the reaction time to 2 weeks and without stirring. After ion-exchange the crystals crashed into tiny platy fragments.

2.4. X-ray crystallography

The crystal structures of $CsHSi_3O_7$ and the proton-exchanged phase were determined from single crystal X-ray diffraction data collected with a Siemens SMART platform diffractometer equipped with a 1 K CCD area detector. A hemisphere of data (1271 frames at 5 cm detector distance) was collected for each phase using a narrow-frame method with scan widths of 0.3° in ω and an exposure time of 30 s/frame. The first 50 frames were remeasured at the end of data collection to monitor instrument and crystal stability, and the maximum correction applied to the intensities was <1%. The data were integrated using the Siemens SAINT program [19], with the intensities corrected for Lorentz factor, polarization, air absorption, and absorption due to variation in the path length through the detector faceplate. Absorption correction was made using the program SADABS [20]. The structures were solved by direct methods and refined on F^2 by full-matrix least squares using SHELXTL [21]. For $CsHSi_3O_7$, all non-hydrogen atoms were refined with anisotropic displacement parameters. The hydrogen atom was located from difference maps and was refined isotropically. The crystal quality deteriorated substantially after ion-exchange. As a result, single crystal X-ray data measured on a suitable fragment of the proton-exchanged phase have a high R_{int} value. Crystal quality deterioration is often observed for ion-exchange and intercalation reactions. For the proton-exchanged phase all silicon atoms were refined anisotropically and the oxygen atoms isotropically. Refinements with anisotropic displacement parameters for the oxygen atoms lead to non-positive definite parameters for some sites. The hydrogen atoms were ignored because of the poor data quality and splitting of the water oxygen atom positions. For comparison the absolute structure of the proton-exchanged phase has been kept the same as $CsHSi_3O_7$, in spite of the high value of the refined absolute structure parameter 1.7(9) for the former. Refinements with a reversed absolute structure model for the proton-exchanged phase showed no change in R-indices. Crystallographic and refinement details are summarized in Table 1. Atom coordinates and selected bond lengths for $CsHSi_3O_7$ are given in Tables 2–4. Further details of the crystal structure investigation can be obtained from the Fachinformationszentrum Karlsruhe, 76344 Eggenstein-Leopoldshafen, Germany, (fax: (49) 7247-808-666; e-mail: crysdata@fiz.karlsruhe.de) on quoting the depository number CSD 413712 and CSD 413713.

2.5. Second harmonic generation measurements

Powder SHG measurements were performed on a modified Kurtz-NLO system [22]. A Continuum Minilite II 1064 nm laser, operating at 1 Hz, was used for all

Table 1
Crystal data and structure refinement details for $CsHSi_3O_7$ and $H_2Si_3O_7 \cdot H_2O$

	$CsHSi_3O_7$	$H_2Si_3O_7 \cdot H_2O$
Formula	H Cs O_7 Si_3	H_4 O_8 Si_3
FW	330.2	216.3
Temperature	293 K	293 K
Space group	$P2_12_12_1$	$P2_12_12_1$
a/Å	4.9115(3)	5.041(2)
b/Å	10.3167(7)	10.507(5)
c/Å	14.1073(9)	13.924(7)
V/Å^3	714.82(8)	737.4(6)
Reflections collected/unique	4386/1645	2613/974
R_{int}	0.0422	0.2131
Data/restraints/parameters	1645/1/105	974/0/64
Goodness-of-fit	1.048	1.220
R indices (all data)	$R_1 = 0.0311$	0.1165
	$wR_2 = 0.0855$	0.2366
Absolute structure parameter	−0.02(2)	1.7(9)

$R1 = \Sigma||F_o| - |F_c||/\Sigma|F_o|$, $wR_2 = [\Sigma(w(F_o^2 - F_c^2)^2)/\Sigma(wF_o^2)^2]^{1/2}$.

Table 2
Atomic coordinates and equivalent isotropic displacement parameters (Å$^2 \times 10^3$) for $CsHSi_3O_7$

	x	y	z	U(eq)
Cs	0.0308(1)	0.0848(1)	0.7471(1)	30(1)
Si(1)	−0.3923(2)	0.2945(1)	0.9436(1)	14(1)
Si(2)	0.0172(2)	−0.0829(1)	0.0089(1)	13(1)
Si(3)	0.5221(2)	−0.1488(1)	0.8930(1)	13(1)
O(1)	0.0529(8)	−0.1961(3)	0.0860(2)	23(1)
O(2)	−0.2916(6)	−0.0745(3)	0.9716(2)	20(1)
O(3)	−0.0855(6)	0.2507(3)	0.9695(2)	21(1)
O(4)	0.2079(7)	−0.1100(3)	0.9179(2)	21(1)
O(5)	0.1018(7)	0.0479(3)	0.0614(3)	21(1)
O(6)	0.4018(7)	0.3837(3)	0.7121(2)	22(1)
O(7)	0.5236(8)	0.2366(3)	0.8431(2)	24(1)
H(1)	0.47(2)	0.297(8)	0.802(6)	80(30)

U(eq) is defined as one third of the trace of the orthogonalized U_{ij} tensor.

Table 3
Atomic coordinates and equivalent isotropic displacement parameters (Å$^2 \times 10^3$) for $H_2Si_3O_7 \cdot H_2O$

	x	y	z	U(eq)
Si(1)	−0.2756(9)	0.2982(3)	0.9468(3)	20(1)
Si(2)	0.131(1)	−0.0826(3)	0.0013(3)	20(1)
Si(3)	0.6309(9)	−0.1595(3)	0.8919(3)	19(1)
O(1)	0.157(3)	−0.1914(9)	0.0825(6)	29(3)
O(2)	−0.167(2)	−0.0809(8)	0.9561(7)	27(3)
O(3)	0.019(3)	0.260(1)	0.9757(7)	32(3)
O(4)	0.336(3)	−0.1098(9)	0.9179(7)	32(3)
O(5)	0.189(2)	0.0506(8)	0.0545(6)	23(2)
O(6)	0.306(2)	0.3584(9)	0.7201(7)	30(3)
O(7)	0.665(3)	0.248(1)	0.8403(8)	39(3)
O(8w*a*)	−0.112(7)	0.082(2)	0.717(2)	44(5)
O(8w*b*)	−0.012(9)	0.081(3)	0.754(3)	44(5)

U(eq) is defined as one third of the trace of the orthogonalized U_{ij} tensor.

Table 4
Selected bond lengths [Å] for $CsHSi_3O_7$

Si(1)–O(7)	1.593(3)
Si(1)–O(3)	1.615(3)
Si(1)–O(3)	1.618(3)
Si(1)–O(5)	1.628(3)
Si(2)–O(5)	1.594(3)
Si(2)–O(1)	1.605(3)
Si(2)–O(2)	1.608(3)
Si(2)–O(4)	1.614(4)
Si(3)–O(6)	1.565(3)
Si(3)–O(2)	1.630(3)
Si(3)–O(4)	1.633(3)
Si(3)–O(1)	1.634(3)
O(7)–H(1)	0.89(2)
O(6)…H(1)	1.59(3)
O(7)…O(6)	2.465(5)
Cs–O(6)	3.025(3)
Cs–O(7)	3.185(4)
Cs–O(7)	3.239(4)
Cs–O(4)	3.256(3)
Cs–O(1)	3.265(4)
Cs–O(5)	3.463(3)
Cs–O(6)	3.522(4)
Cs–O(6)	3.616(3)
Cs–O(3)	3.620(3)

measurements. Because the SHG efficiency of powders has been shown to depend strongly on the particle size [23], the samples were ground and sieved into distinct particle size ranges, <20, 20–45, 45–63, 63–75, 75–90, and 90–125 μm. To make relevant comparisons with known SHG materials, polycrystalline quartz was also ground and sieved into the same particle-size ranges. All of the powders were placed in separate capillary tubes. The SHG light, i.e., 532 nm green light, was collected in reflection and detected by a photomultiplier tube (Oriel Instruments). To detect only the SHG light, a 532 nm narrow band-pass interference filter was attached to the tube. A digital oscilloscope (Tektronix TDS 3032) was used to view the SHG signal.

3. Results and discussion

3.1. The crystal structure

$CsHSi_3O_7$ crystallizes in the orthorhombic system with space group symmetry $P2_12_12_1$. There are three different tetrahedral silicon sites (Fig. 1). Si(1) and Si(3) are each bonded to three bridging oxygen atoms and a terminal oxygen atom, while Si(2) is bonded to four bridging oxygen atoms. The terminal oxygen atom O(7) of the the $Si(1)O_4$ tetrahedron is bonded to a proton to form a silanol group. The shortest Si–O bond length

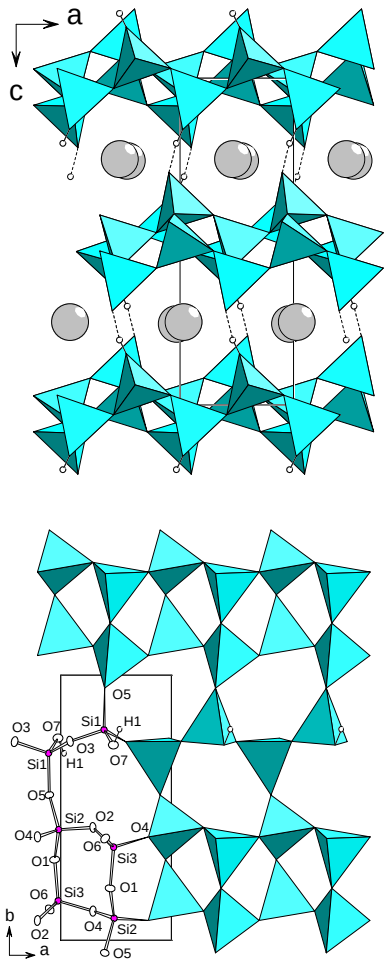

Fig. 1. The structure of $CsHSi_3O_7$ viewed along [010] (top) and the HSi_3O_7 layer (bottom). Dashed lines represent hydrogen bonds. Gray circles represent Cs atoms.

(1.565 Å) is found, as expected, for the terminal Si(3)–O(6) bond. The $Si(2,3)O_4$ tetrahedra are linked to form 4-member rings that are interconnected to form double chains parallel to [100], while the $Si(1)O_4$ tetrahedra are linked to form single chains also along [100]. The single chains of $Si(1)O_4$ tetrahedra and the double chains of $Si(2,3)O_4$ tetrahedra are cross-linked alternatively to form a single layer by sharing the O(5) corners. Six-ring voids are outlined by the linking of the single and double chains. The single layers are stacked along the [001] direction and neighboring layers are related by 2_1 screw axes. Very short hydrogen bonds occur between the terminal silanol groups of one layer and the terminal O(6) atoms of the neighboring layers (O(6)…O(7): 2.465 Å, Table 4). The negative charge of the HSi_3O_7 single layers is balanced by the interlayer Cs^+ cations. There are nine oxygen atoms surrounding the Cs atom with Cs–O distances in the range 3.025–3.620 Å. The three shortest Cs–O bonds are formed with the terminal O(6) and O(7) atoms. The CsO_9 polyhedron is highly irregular with the Cs atom strongly shifted from the center to one side.

The double chains of the Si_3O_7 layer in $CsHSi_3O_7$ are also found in the recently reported one-dimensional structure of $CsHSi_2O_5$ (Fig. 2d) [11]. The closely related compounds $KHSi_2O_5$ [24] and $NaHSi_2O_5 \cdot 2H_2O$ [25] have silicate layers that may be considered as forming from cross-linking only the single chains of $CsHSi_3O_7$. In the Si_3O_7 layer of $CsHSi_3O_7$ the ratio of single chains to double chains is 1:1. By varying this ratio a series of layered silicate anions with the general formula $(Si_4O_9)_m(Si_2O_5)_n$ may be generated. The Si_3O_7 layer represents the member of the series with $m = n = 1$. The Si_2O_5 layer of $KHSi_2O_5$ is an end member with $m = 0$, $n =$ infinite. The other end member layer with $m =$ in- $=$ infinite, $n = 0$, is found in the layered structure of $K_2Si_4O_9$ [26] in which the double chains are directly linked to each other to form one column of 6-rings between neighboring double chains (Fig. 2c). The ratio of 6- to 4-rings in the layers of each member of the series is $(m+n)/(2m)$ while the ratio of 4- and 3-connected tetrahedra (Q^4/Q^3) equals to $m/(m+n)$. The general formula should be helpful in finding new materials since the layer structure and charge of each member of the series is readily predicted.

Strong hydrogen bonds ($d_{(O\ldots O)} < 2.50$ Å) [27] are also found in the structures of $AHSi_2O_5$, $A =$ K, Cs [11,24]. A common feature in these two compounds and $CsHSi_3O_7$ is that the oxygen atoms forming the hydrogen bonds are terminal corners of three-connected SiO_4 tetrahedra. According to a statistical study of silicate minerals containing silanol groups, Si–OH bond length decreases as the connectedness of the SiO_4 tetrahedron increases [28]. In three-connected tetrahedra the Si–OH bonds tend to be shorter than the three bridging Si–O bonds. The shorter Si–OH bond implies that the more negative charge of the O atom is polarized towards Si, thus increasing the tendency of the OH group to form strong hydrogen bond. On the other hand, the residual charge of the terminal O^{2-} corners of the SiO_4 tetrahedra is large, and is not readily balanced by the large monovalent cations in these structures. Therefore, both the terminal O atom and the OH group in these structures favor strong hydrogen bonds. The O–H…O

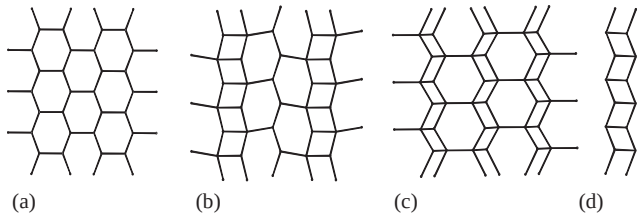

Fig. 2. Structures of the layer series $(Si_4O_9)_m(Si_2O_5)_n$. (a) The layer of $KHSi_2O_5$ with $m = 0$, $n =$ infinite, (b) the layer of $CsHSi_3O_7$ with $m = n = 1$, (c) the layer of $K_2Si_4O_9$ with $m =$ infinite, $n = 0$, and (d) the double chain of $CsHSi_2O_5$. Each node represents a SiO_4 tetrahedron.

angle in $CsHSi_3O_7$ is very close to the average value of 167° found in other inorganic structures [28].

3.2. Ion-exchange

Preliminary experiments showed that at room temperature the Cs^+ cations of $CsHSi_3O_7$ are not readily exchanged by protons. However, at 100°C the ion-exchange process occurs easily. After proton ion-exchange, elemental analysis gave 1.68% H, 39.69% Si and <0.29% Cs. The results show almost complete removal of the Cs^+ cations (<0.002 Cs per Si atom) and correspond to the composition $H_2Si_3O_7 \cdot H_2O$ (calc. 1.85% H, 39.01% Si). The powder X-ray diffraction patterns measured before and after ion-exchange were compared with the simulated patterns. As shown in Fig. 3, the agreement between observed and simulated patterns is good. The simulated patterns were calculated from single crystal structure data with the program PowderCell [29]. Preferred orientation along the (001) plane was apparent and was compensated in the simulated patterns for both phases [30]. The crystal structure of $H_2Si_3O_7 \cdot H_2O$ determined from single crystal data is essentially the same as $CsHSi_3O_7$ with interlayer water molecules occupying the original Cs positions (Fig. 4). The Si(3)–O(6) bond length increases from 1.565 Å in $CsHSi_3O_7$ to 1.603 Å in $H_2Si_3O_7 \cdot H_2O$ due to protonation of the terminal O(6) atom. The O(6)…O(7) distance increases from 2.465 Å in $CsHSi_3O_7$ to 2.72 Å in $H_2Si_3O_7 \cdot H_2O$, indicating significant weakening of the interlayer hydrogen bonds in the latter. The interlayer water oxygen site of $H_2Si_3O_7 \cdot H_2O$ is split into two positions O(8wa) and O(8wb) which are 0.72 Å apart from each other with occupancies 0.58(4) for O(8wa) and 0.42(4) for O(8wb). Both water oxygen positions are at favorable distances to form hydrogen bonds to the terminal O(6) and O(7) atoms (Fig. 4b).

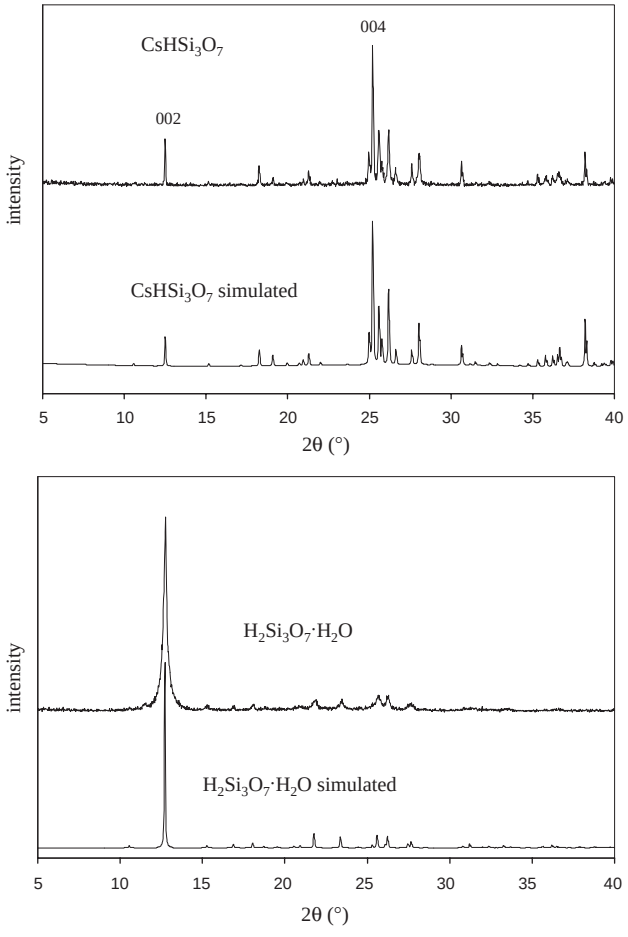

Fig. 3. Observed and simulated powder X-ray diffraction data for $CsHSi_3O_7$ (top) and $H_2Si_3O_7 \cdot H_2O$ (bottom). Preferred orientation along (0 0 1) was compensated for the simulated patterns [29,30].

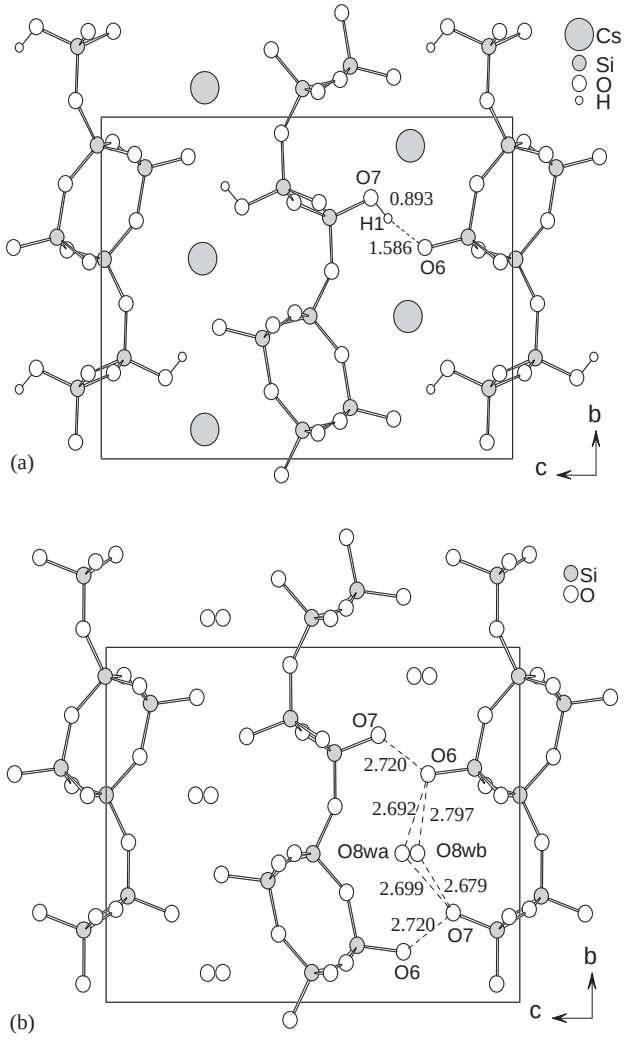

Fig. 4. The structure of $CsHSi_3O_7$ (a) and $H_2Si_3O_7 \cdot H_2O$ (b) viewed along [100]. Atom distances are marked in angstroms.

3.3. TGA

TAG data measured between 30°C and 1000°C for the proton-exchanged sample show a sharp weight loss that starts immediately upon heating and ends at ~120°C. A second weight-loss starts at ~250°C and ends at ~650°C. The observed weight-loss of 8.39% below 120°C corresponds to dehydration of the sample (theor. 8.33% for $H_2Si_3O_7 \cdot H_2O$). The total weight-loss of 6.8% between 250°C and 650°C is less than the theoretical value of 8.33% for a complete dehydroxylation, indicating that part of the hydroxyl groups were trapped in the residue. The residue was shown to be amorphous by powder X-ray diffraction. Infrared data measured for the residue show a weak broad band at 3435 cm^{-1} due to the stretching vibrations of the trapped OH groups. Si–OH groups have been observed in silicate glasses treated at temperatures over 1000°C [31]. A proton-exchanged sample heated at 150°C for 45 min was examined with X-ray powder diffraction. The diffraction patterns were closely similar before and after heating, which indicates that dehydration did not cause substantial changes of the structure.

TGA data for $CsHSi_3O_7$ show a sharp weight loss of 2.2% between 500°C and 600°C. The residue was shown to be amorphous by powder X-ray diffraction data. The observed weight loss is less than the theoretical value of 2.73% for a complete dehydroxylation, due to retention of some Si–OH groups in the residue.

3.4. Spectroscopy

Fig. 5 shows the infrared spectra for both the original and the proton-exchanged samples. For $CsHSi_3O_7$ the strong bands in the region 950–1300 cm^{-1} are usually believed to be due to asymmetric stretching vibrations of Si–O–Si linkages and stretching vibrations of terminal Si–O bonds. The bands between 400 and 800 cm^{-1} are associated with the symmetric stretching vibrations of Si–O–Si bridges [32]. For strong O–H…O hydrogen bonds v(OH) shifts to low wave number regions as the O…O distance decreases. The v(OH) band of $CsHSi_3O_7$ is expected in the range 800–1200 cm^{-1} from the short O(7)…O(6) distance of 2.465 Å [27], which is not resolved from Si–O vibration bands. For the proton-exchanged sample $H_2Si_3O_7 \cdot H_2O$ the bending mode of water molecules is observed at 1624 cm^{-1}. Stretching vibrations of OH groups v(OH) are observed between 3000 and 3700 cm^{-1}. The broad low frequency bands are related to the disordered interlayer water molecules. The sharp high frequency band at 3658 cm^{-1} can be assigned to the terminal OH groups that are involved in much weakened hydrogen bonding [32,33].

The UV-Vis-NIR diffuse reflectance spectra are shown in Fig. 6. The absorption band observed in the spectrum of $H_2Si_3O_7 \cdot H_2O$ at ~1400 nm (7150 cm^{-1}) is related to the first overtone of the fundamental stretching vibration of the hydroxyl groups. The absorption bands near 1900 nm are associated with combinations of bending and stretching vibrations of water molecules [34].

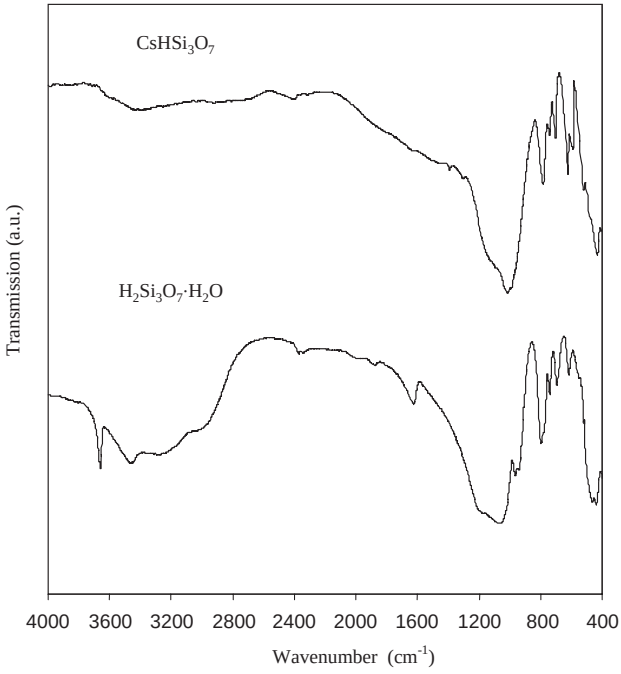

Fig. 5. The infrared spectra of $CsHSi_3O_7$ and $H_2Si_3O_7 \cdot H_2O$.

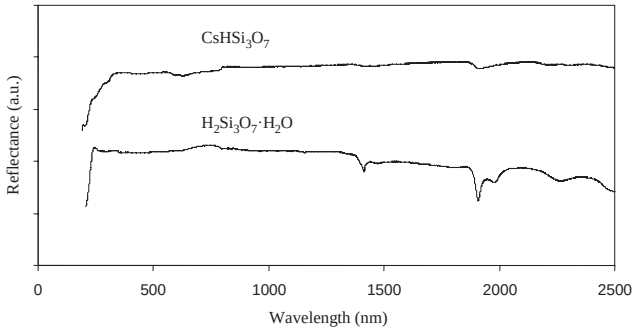

Fig. 6. The diffuse reflectance spectra of $CsHSi_3O_7$ and $H_2Si_3O_7 \cdot H_2O$.

3.5. Second-order NLO properties

Powder SHG measurements on sieved polycrystalline $CsHSi_3O_7$ revealed a SHG efficiency comparable to that of quartz. For a non-phase-matchable material the SHG intensity decreases as the particle size becomes substantially larger than the coherence length of the materials. As can be seen from Fig. 7, both $CsHSi_3O_7$ and the proton-exchanged phase $H_2Si_3O_7 \cdot H_2O$ are not phase-matchable. The SHG active feature of $H_2Si_3O_7 \cdot H_2O$ confirms that the ion-exchange process did not destroy

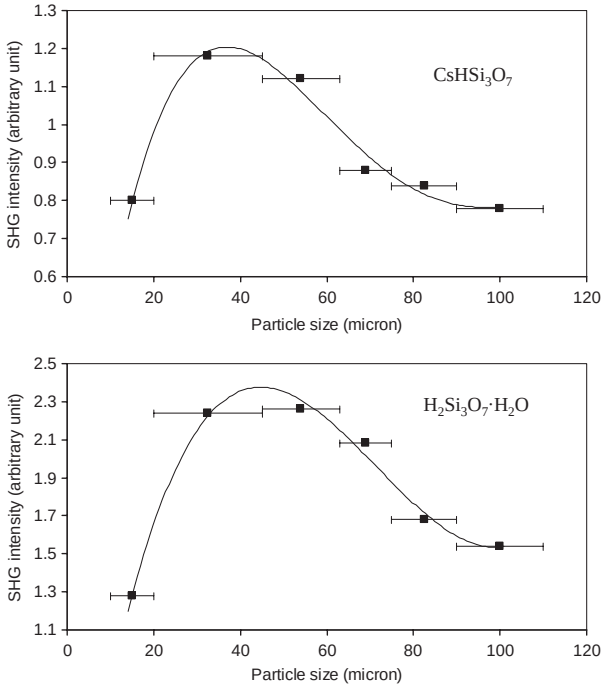

Fig. 7. SHG data for $CsHSi_3O_7$ (top) and $H_2Si_3O_7 \cdot H_2O$ (bottom).

the non-centrosymmetric character of the original structure.

Acknowledgments

We thank Dr. P. S. Halasyamani and Dr. K. Ok for their help in the SHG measurements and the National Science Foundation (DMR-0120463), the R.A. Welch Foundation for financial support. This work made use of Shared Experimental Facilities of the Center for Materials Chemistry (CMC-UH) at the University of Houston.

References

[1] E. Ruiz-Hitzky, J.M. Rojo, Nature 287 (1980) 28.
[2] A.J. Jacobson, in: A.K. Cheetham, P. Day (Eds.), Solid State Chemistry: Compounds, Oxford University Press, New York, 1992, p. 182.
[3] G. Alberti, U. Costantino, Comprehensive Supramol. Chem. 7 (1996) 1.
[4] I. Khan, D. O'Hare, J. Mater. Chem. 12 (2002) 3191.
[5] P.S. Halasyamani, K.R. Poeppelmeier, Chem. Mater. 10 (1998) 2753.
[6] J. Gopalakrishnan, K. Ramesha, K.K. Rangan, S. Pandey, J. Solid State Chem. 148 (1999) 75.
[7] K. Kuroda, K. Hiraguri, Y. Komori, Y. Sugahara, H. Mouri, Y. Uesu, Chem. Commun. (1999) 2253.
[8] I. Fujita, K. Kuroda, M. Ogawa, Chem. Mater. 15 (2003) 3134.
[9] D. Mochizuki, A. Atsushi, K. Kuroda, J. Am. Chem. Soc. 124 (2002) 12082.
[10] T.C. Chao, D.E. Katsoulis, M.E. Kenney, Chem. Mater. 13 (2001) 4269.
[11] G. Dorsam, V. Kahlenberg, R.X. Fischer, Z. Anorg. Allg. Chem. 629 (2003) 981.
[12] S. Rakic, V. Kahlenberg, B.C. Schmidt, Z. Kristallogr. 218 (2003) 413.
[13] F. Kooli, F. Mizukami, Y. Kiyozumi, Y. Akiyama, J. Mater. Chem. 11 (2001) 1946.
[14] G.G. Almond, R.K. Harris, K.R. Franklin, J. Mater. Chem. 7 (1997) 681.
[15] F. Liebau, Structural Chemistry of Silicates, Springer, Berlin, 1985.
[16] X. Wang, L. Liu, A.J. Jacobson, Angew. Chem. Int. Ed. 42 (2003) 2044.
[17] X. Wang, J. Huang, A.J. Jacobson, J. Am. Chem. Soc. 124 (2002) 15190.
[18] X. Wang, L. Liu, A.J. Jacobson, J. Am. Chem. Soc. 124 (2002) 7812.
[19] SAINT, Program for Data Extraction and Reduction, Siemens Analytical X-ray Instruments Inc., Madison, USA, 1996.
[20] G.M. Sheldrick, SADABS, Program for Siemens Area Detector Absorption Corrections, University of Gottingen, Germany, 1997.
[21] G.M. Sheldrick, SHELXTL, Program for Refinement of Crystal Structures, Siemens Analytical X-ray Instruments Inc., Madison, USA, 1994.
[22] S.K. Kurtz, T.T. Perry, J. Appl. Phys. 39 (1968) 3798.
[23] J.P. Dougherty, S.K. Kurtz, J. Appl. Crystallogr. 9 (1976) 145.
[24] Y.A. Malinovskii, N.V. Belov, Dokl. Akad. Nauk SSSR 246 (1979) 99.
[25] H. Annehed, L. Falth, F.J. Lincoln, Z. Kristallogr. 159 (1982) 203.
[26] H. Schweinsberg, F. Liebau, Acta Crystallogr. B30 (1974) 2206.
[27] G.A. Jeffrey, An Introduction to Hydrogen Bonding, Oxford University Press, Oxford, 1997.
[28] D. Nyfeler, T. Armbruster, Amer. Mineralog. 83 (1998) 119.
[29] W. Kraus, G. Nolze, J. Appl. Crystallogr. 29 (1996) 301.
[30] H. Toraya, F. Marumo, Mineral. J. 10 (1981) 211.
[31] A. Baraldi, R. Capelletti, N. Chiodini, D. Oppici, R. Scotti, A. Vedda, Radiat. Eff. Def. Solids 157 (2002) 1139.
[32] Y. Huang, Z. Jiang, W. Schwieger, Chem. Mater. 11 (1999) 1210.
[33] R.H.A. Ras, C.T. Johnston, E.I. Franses, R. Ramaekers, G. Maes, P. Foubert, F.C. De Schryver, R.A. Schoonheydt, Langmuir 19 (2003) 4295.
[34] P.M. Bell, H.K. Mao, G.R. Rossman, in: C. Karr (Ed.), Infrared and Raman Spectroscopy of Lunar and Terrestrial Minerals, Academic Press Inc., New York, 1975.